Progress in Photovoltaics: Research and Application 23, 1929 (2015)

Monolithically interconnected lamellar Cu(In,Ga)Se_2 micro solar cells under full white light concentration

Bernhard Reinhold[*1], Martina Schmid[1,5], Dieter Greiner[2], Manuel Schüle[3], David Kieven[4], Ahmed Ennaoui[4], Martha Ch. Lux-Steiner[4,5]

[1]Helmholtz-Zentrum Berlin für Materialen und Energie, Nanooptical Concepts for PV, Hahn-Meitner-Platz 1, 14109-Berlin, Germany

[2]Helmholtz-Zentrum Berlin für Materialen und Energie, Institute for Technology, Hahn-Meitner-Platz 1, 14109-Berlin, Germany

[3]HTW-Berlin - University of Applied Sciences, Wilhelminenhofstr.75a, 12459-Berlin, Germany

[4]Helmholtz-Zentrum Berlin für Materialen und Energie, Institute for Heterogeneous Material Systems, Hahn-Meitner-Platz 1, 14109-Berlin, Germany

[5]Freie Universität Berlin, Department of Physics, Arnimallee 14, 14195-Berlin, Germany

*Corresponding author: Bernhard Reinhold, E-mail: Bernhard.reinhold@helmholtz-berlin.de

Keywords: solar cell, micro concentrator, chalcopyrite, light concentration, CPV

Abstract:

Thin film solar cells already benefit from significant material- and energy savings. By using photon management, the conversion efficiency and the power density can be enhanced further, including a reduction of material costs. In this work, micrometer-sized Cu(In,Ga)Se_2 (CIGS) thin film solar cells were investigated under concentrated white light illumination (1-50x). The cell design is based on industrially standardized, lamellar shaped solar cells with monolithic interconnects (P-scribe). In order to characterize the shunt- and series resistance profiles and their impact on the device performance the cell width was reduced stepwise from 1900 to 200 µm and the P1-scribe thickness was varied between 45 and 320 µm. The results are compared to macroscopic solar cells in standard geometry and dot-shaped microcells with ring contacts. Under concentrated white light, the maximal conversion efficiency could be increased by more than 3.8% absolute for the lamellar microcells and more than 4.8% absolute in case of dot-shaped microcells compared to their initial values at 1 sun illumination. The power density could be raised by a factor of 51 and 70, respectively. But apparently, the optimum concentration level and the improvement in performance strongly depend on the chosen cell geometry, the used contact method and the electrical material properties. It turns out, that the widely used industrial thin film solar cell design pattern cannot simply be adapted to prepare micro-concentrator CIGS solar modules, without significant optimization. Based on the experimental and simulated results, modifications for the cell design are proposed.

1. Introduction

In comparison to a silicon wafer based solar cell technology, the thin film solar cell production benefits from production processes with lower cost and higher savings in materials and energy demand. A common feature for all thin film solar cells, like Cadmium telluride, Chalcopyrite or Kesterite, is a film thickness below 5 µm and processing temperatures that typically do not exceed 950 K [1,2]. In the recent years thin film solar cells and polycrystalline chalcopyrite absorbers in particular showed their ability to compete with polycrystalline silicon based solar cells. Lab based Cu(In,Ga)SSe record solar cells surpass with a conversion efficiency of 21.7% already the world record for polycrystalline silicon solar cells [3,4].

To optimize photovoltaic devices further new technological enhancements are necessary. One potential and promising way is the implementation of photon managing elements, like light guiding structures [5,6], spectral converter layers [7] or light concentrating lenses [8-15]. By combining light concentrating elements with solar cells, the cell area and hence the used absorber material can be reduced by 1 to 2 orders of magnitude without power loss. In addition, the conversion efficiency can be increased due to the photon flux driven enhancing of the open circuit voltage. But, contrary to conventional light concentrating strategies that typically focus on high concentration level between 200 and 500 suns, what finally results in high efforts for large Fresnel lenses, bulky module concepts and an obligatory 2-axis sun tracking, the new and emerging topic of micro-concentrator cells focuses on very small solar cells in a micrometer range combined with low concentrating optics.

The microcell approach offers several advantages. Beside potentially lower cost for lenses, larger acceptance angles, reduced requirements for tracking systems and a more compact module design, new material classes of light absorbing materials can enter this field [8,14]. The within 1-2 order of magnitude reduced cell dimensions lowers the demands in bulk- and contact resistivity and the increased surface aspect ratio can favor the heat dissipation [8-12, 14]. It is further assumed, that the thereby possible large oversizing of the focal spot in comparison to the active cell area will significantly lower the demands in sun tracking, that can be in principle already reduced to a one-axis tracking in case of lamellar microcells in combination with cylindrical lenses. As a consequence of the lower production costs for thin film solar cells and the potentially saved system requirements, like multi-axis tracking, the final economically reasonable cell- and module efficiency decouples from recent references known for GaAs- and InGaP-based multi-junction CPV-systems pending between 39-46.0% and 30-40%, respectively [3].

First publications in the field of a microcell approach base on light absorbing materials like silicon or gallium-arsenide, that have been achieved by J.A. Rogers and M. Kanayama et al. [14,16,17]. For Cu(In,Ga)Se_2-based absorber material M. Paire and D. Lincot et al. investigated and published an enhancement in conversion efficiency by 4% absolute at 120x light concentration, that were recently further improved to 21.3% including a plus of 5% absolute at 475x concentration [11,12]. J.S.Ward et al. published for light concentration experiments with Cu(In,Ga)Se_2-absorber a maximum conversion efficiency of 23.3% at 15x concentration, corresponding to a gain of 5.4% absolute [18]. Theoretical calculations even predict a plus in conversion efficiency of 15% absolute at 46.200x concentration [8]. Low concentrator concepts based on solar modules also exist [19,20], but will not be discussed in this article.

Caused by the fact, that most of the recent work about chalcopyrite based micro cells focuses on basic theoretical studies and a dot-shaped microcell design [8-12], we orientated our work on lamellar shaped Cu(In,Ga)Se_2 solar cells equipped with an industrially already implemented monolithic interconnection type. In order to track changes in the cell performance from macro- to microcells, the

lateral cell dimension was reduced stepwise from 1900 to 200 µm, including an adjustment of the P1-scribe width between 45 and 320 µm (fig.1). To classify the findings against other contact design setups, the results were finally compared to dot-shaped microcells of similar size and to macroscopic reference cells equipped with a ring- and a finger-like grid, respectively.

2. Principles of solar cell performance under concentrated light

The current-voltage characteristics of pn-junction based solar cells can be described by the single diode equation (1.1) [21].

$$I = I_{ph} - I_0(e^{\frac{U+I*R_s}{n*U_T}} - 1) - \frac{U + I * R_s}{R_p} \qquad 1.1$$

According to equation 1.1, the current I depends on the applied voltage U, the light induced photocurrent I_{ph}, the saturation dark current I_0, the diode factor n, the series resistance R_s, the parallel resistance R_p and the thermal voltage $U_T = (k_B*T/q)$, with T the temperature , q the elementary charge and k_B the Boltzmann constant. Since the photocurrent of a solar cell depends not only on the spectral response of the light absorbing material but also on the given photon flux, the photocurrent and thus the short circuit photocurrent I_{sc} will rise with concentrated light. This relation can be written in a good approximation for cells with low series resistance, assuming constant spectral conditions and negligible changes in trap occupation with concentration by introducing the concentration factor C in equation 1.2 as ratio of the short current density at concentrated light and standard test conditions (1000 W/m^2).

$$I_{sc}^{CPV} = C * I_{sc}^{STC} \qquad 1.2$$

With ascending light intensities, the open circuit voltage of the device U_{oc} will also increase due to the enhanced Fermi level shift. Resolving equation 1.1 for the voltage U together with the assumption of negligible resistances, leads to equation 1.3, where the U_{oc} increases with the logarithm of the concentration factor C.

$$U_{oc} = (n * U_T) * \ln\left(\frac{(C * I_{sc}^{STC})}{I_0} + 1\right) \qquad 1.3$$

$$\eta = \frac{P_{mp}}{P_{light}} = \frac{FF * U_{oc} * I_{sc}}{P_{light}} \qquad 1.4$$

Following now eq. 1.4, the maximum cell power P_{mp} as well as the conversion efficiency η will also rise under concentrated light, presupposed that their dependency on the parameters T, I_0, n, R_s and R_p does not start to alter the device performance.
The fill factor FF reflects the influence of these parameters in a combined form [22-24]. Therefore we focus on the FF to simulate the cell power and conversion efficiency, described in more detail later in chapter 4.3. Based on a publication of D.L. Pulfrey et al., the dependency of the FF on the series resistance R_s can be expressed by equation 1.5 [22]. The photocurrent value I_{mp}, present at the

maximum power point, is calculated iteratively by using equation 1.6. This relation can be obtained by resolving eq. 1.1 for *U* and differentiating the power *P* for the current *I*, assuming in this first basic approach infinitively high parallel resistances [22,25].

$$FF = \frac{U_{mp} * I_{mp}}{U_{oc} * I_{sc}} = \frac{I_{mp}^2}{U_{oc} * I_{sc}} * \left[\frac{n * U_T}{(I_{ph} + I_0 - I_{mp})} + R_s \right] \qquad 1.5$$

$$I_{mp} = n * U_T * \left[\ln\left(\frac{I_{ph} + I_0 - I_{mp}}{I_0} \right) - \frac{I_{mp}}{I_{ph} + I_0 - I_{mp}} \right] \Big/ 2 * R_s \qquad 1.6$$

Combining now the equations 1.2, 1.3, 1.5 and 1.6, the maximum cell power P_{mp} and hence the light to electricity conversion efficiency η can be calculated by using equation 1.4.

3. Experimental

The $Cu(In,Ga)Se_2$ layer were deposited onto a molybdenum coated soda lime glass in a multistage co-evaporation process with a Cu-rich phase during the film growth [26]. On top of the $Cu(In,Ga)Se_2$ a 25 nm thick CdS and a 130 nm thick i-ZnO layer were deposited. The solar cells were completed after sputtering 850 nm ZnO:Al on top. Macroscopic cells with 0.5 cm^2 active area and a standard, finger-like Ni:Al contact grid were prepared as references. Their averaged cell efficiency of 15.6 % at 1 sun is comparable to recent performance standards, in that the $Cu(In,Ga)Se_2$ solar cells were aligned for an application in solar modules [3]. No sodium or potassium based post-treatment was applied. A schematic view of the lamellar solar cell geometry and contact pattern is shown in figure 1. The light concentrator unit could be realized by cylindrical, plano-convex lenses in principle. The solar cells design pattern, which is widely used in industrial applications, consists of two major areas: the active cell area zone (ACW) and the interconnection zone (ICW). The ICW includes three patterning structures named as P1-, P2- and P3-scribe, what allows a serial connection of single solar cells to form a solar module with defined current and voltage. The used monolithic contact design is implemented by dividing the molybdenum back contact with a P1-scribe first, followed by a P2-scribe into the $Cu(In,Ga)Se_2$ layer and a final P3-scribe, that separates the front-contact between two cells.

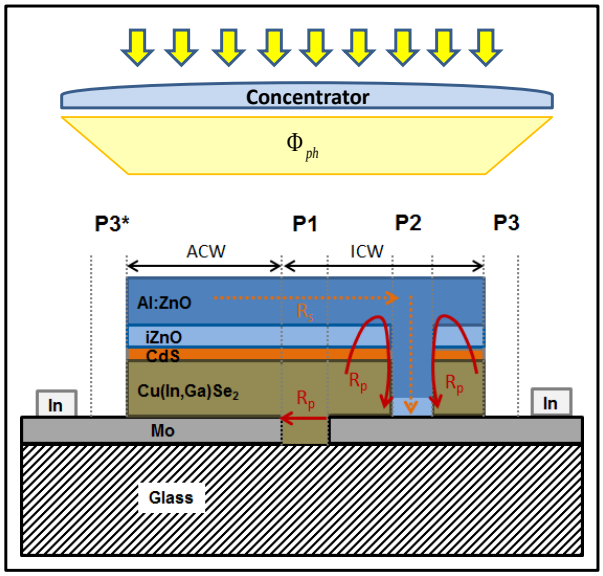

Figure 1: Cross section of the investigated lamellar $Cu(In,Ga)Se_2$ solar cells. The most relevant series- and parallel resistances are sketched.

The pre-patterning of the molybdenum layer was performed using a laser scribing tool from Rofin Basel Lasertech operated at 1064 nm wavelength (P1-scribe). Four different sets of P1-scribe widths were created: 45 µm (A-series), 70 µm (B-Series), 160 µm (C-series) and 320 µm (D-series). The lateral distance of the interconnection zone (ICW) increases therefore from 242 to 554 µm (fig. 1). Other dimensions in the ICW-zone, like the P1P2-distance (80 µm), the mechanically structured P2- and P3-scribes (40 µm) and the P2P3-distance (80 µm) were kept constant for all cells. Changes in the P2- and P3-scribe are assumed to be non-relevant for the cell performance, because of the already large geometrical factor between TCO-layer thickness and P2-scribe width (47.1x) and the beneficial isolation in air between different cells. The interstices between the scribes were chosen to be as low as technically realizable to minimize losses in series resistance. The cell length was 11 mm for experiments at standard test conditions (STC) and 3 mm for light concentrating experiments. In the experiment, the lateral cell width ACW was reduced successively in five steps from 1900 to 1500, 1000, 500 and finally to 200 µm. Hence, the active cell area decreased from 0.220 to 0.020 cm^2. By using circular masks, dot-shaped microcells were prepared from planar stacks of Mo/CIGSe/CdS/iZnO/Al:ZnO by depositing a conductive Ni:Al-layer on top. Three different cell sizes of exposed CIGS with radii of 2150, 1550 and 750 µm were prepared and investigated. The results were adducted to balance and support the investigations for the lamellar microcells that are primary focused in that publication. More information about the dot-shaped micro cells itself will be published soon in an additional publication.

The electrical cell properties were measured with a WACOM class AAA sun simulator combined with an actively cooled sample holder. All cells were characterized first at standard test conditions (STC: 298.15 K, AM 1.5 spectrum ASTM-G 173, 1000 W/m^2). The concentration of light was implemented by using spherical lenses that were optimized for low reflection and low spherical and chromatic aberrations (25-75 mm diameter, plan-convex, MgF_2 coating, 25-150 mm focal length, Edmund Optics). The focal length was varied in such a way, that the focal point was always larger than the cell dimension. If not stated differently, all current voltage characteristics are related to the active cell area (AA), without considering the area of the interconnection zone (ICW). To determine the active and total cell area an Olympus BH2-UMA light microscope (50x magnification) was used. The area based uncertainty in cell power and efficiency, mainly caused by the edge formation during the mechanical

scribing processes and the limited optical resolution of the microscope, is estimated to be +/- 3% for the lamellar and +/-5% for the dot-shaped microcells.

The light concentration was estimated by two different methods. In the first method, the ratio between I_{sc} obtained for concentrated light and at standard test conditions (I_{sc}-CPV / I_{sc}-STC) is used. This procedure bases on the relation of a linear rise of the short circuit current with increasing light concentration. The range of validity depends on the cells series resistance. In the limitation regime, the short circuit currents will be determined too low, resulting in under-estimated concentration levels. In the second approach, the light intensity was determined by using neutral density filters of different attenuations (ND-Filter with AR-Coating, type: NE-03B/05B/10B/20B, Thorlabs). After shading the cell with the ND-filter, the incoming light was re-focused until the initial IV-parameter observed for STC-conditions could be achieved again. With the known attenuation of the ND-filter, estimated before in transmission- and reflection measurements (Perkin Ellmer, Lamda 950, 300-2000 nm), the light intensity could be recalculated without any interfering electrical effects on the cell. The temperature of the cell layer stack was measured with two thermocouples. One was positioned in the actively cooled copper substrate plate. The other was fixed on top of a test solar cell by silicon rubber in close contact to the light focus area. Caused by the active cooling (set-point: 298.15 K) and the natural thermal emission the overall cell temperature rose weakly in the concentration experiments from 298 to 319 K at 1 and 36 suns, respectively. The experimental temperature data were fitted by using a power law function ($T=23.9*C^{0.2}$, R^2: 0.997) in order to derive the temperature for any random concentration level. For the temperature based corrections of the open circuit voltage a temperature coefficient of -0.239 %/K was considered [27].

4. Results and Discussion

4.1 Lamellar micro cells at standard test conditions (STC)

In figure 2, the current voltage characteristics of differently sized lamellar solar cells from series A are compared to a 0.5 cm^2 sized macroscopic reference cell with a finger-like contact grid. Compared to the reference and with decreasing active area width (ACW) in particular, the IV-performance and hence the conversion efficiency deteriorates. This trend is caused by a decline in U_{oc} and *FF* that averaged values decrease from 594 to 559 mV and from 74 to 70% just by changing the contact method. The values dropped further from 559 to 543 mV and from 70 to 42% after reducing the cell width from 1900 to 200 µm. Thus, the averaged conversion efficiency decreased from 13.7% for 1900 µm sized cells to less than 6.4% for the 200 µm sized microcells out of series A (table 1). Apparently, a new situation appears for the micrometer sized monolithically interconnected solar cells. It seems that the cell performance is strongly affected by changed influences of series- and parallel resistances.

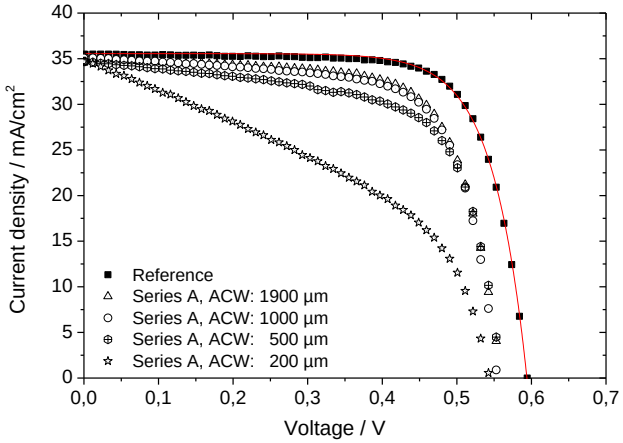

Figure 2: IV-characteristics of differently sized lamellar microcells in comparison to a macroscopic reference with a finger-like contact grid.

This is supported by analyzing the effect of an increasing P1-scribe width on the IV-characteristics. For large microcells, one could recognize only a minor beneficial effect in re-increasing open circuit voltages (+3.9%) and fill factors (+2.0%), when the P1-scribe width was increased from 45 to 320 µm. But for microcells below 1000 µm ACW, the improvements were significantly higher, reaching in maximum plus +6.2% for the U_{oc} and +26.3% relative for the *FF*. The experiments also revealed that the dimension of the P1-scribe influences the short circuit photocurrent I_{sc} of the cells. Within the series A to D an overall increase of 4.7% could be observed. The area related contribution in I_{sc} was estimated to be 32.2 mA/cm^2 in case of 45 µm sized P1-scribes and lowered to 12.1 mA/cm^2 for 320 µm sized P1-scribes. Limits in the diffusion length of charge carrier and the lateral drop of electrical fields are assigned for the different activity. For efficiency calculations, the P1-scribe related gain in I_{sc} was considered to preserve the comparability. The expected I_{sc}-contribution of the P1P2-zone could not be verified by space resolved photocurrent measurements.

In table 1 one can see these trends expressed by the active area based conversion efficiency. The smaller the cell size, the more important and beneficial is a large P1-scribe width for the U_{oc} and *FF* and hence a good efficiency. The beneficial effect is assigned to an improved electrical isolation between back- and front contact. Whereas the efficiency increased for macroscopic 1900 µm ACW cells from 13.7 to 14.4% in series A to D, the efficiency rose from 6.4 to 9.% in case of 200 µm ACW. This corresponded to a relative change of 4.8 to 28%, respectively. However, for 200 µm ACW cells, the efficiency was pinned below 10% for all investigated P1-scribe dimensions, indicating that this method to improve internal parallel resistances does not explain all changes in case of microcells.

Table 1: Averaged conversion efficiency for different cell- and interconnect geometries at 1 sun.

Averaged conversion efficiency, active area, [%]	≥ 14.0	13.9-11.5	11.4-9.0	8.9-6.5	≤ 6.4

P1 / ACW	A-series 45 µm	B-series 75 µm	C-series 160 µm	D-series 320 µm		Dot-Cells -	P1 / ACW
1900 µm	13.7 +/-0.06	14.5 +/-0.11	14.7 +/-0.08	14.4 +/-0.03		16.0 +/-0.17	**2150 µm**
1500 µm	13.8 +/-0.05	14.0 +/-0.06	14.3 +/-0.18	14.4 +/-0.05		15.7 +/-0.90	**1550 µm**
1000 µm	13.1 +/-0.09	13.9 +/-0.06	13.5 +/-0.20	13.6 +/-0.05		-	-
500 µm	11.4 +/-0.24	12.2 +/-0.10	11.8 +/-0.27	12.2 +/-0.12		13.6 +/-0.19	**750 µm**
200 µm	6.4 +/-0.11	7.7 +/-0.09	7.4 +/-0.10	9.1 +/-0.10		-	-
Reference cells Grid, 0.5 cm²	15.6 +/-0.22					16.5 +/-0.20	**Reference cells Grid, 0.5 cm²**

A similar trend was observed for the dot-shaped microcells (table 1). Reducing the radius of the active cell area together with fixed dimensions for the contact area led the averaged *FF*-values and hence the conversion efficiency drop from 16.0 to 13.6% in case of 2150 µm and 750 µm ACW dot-cells, respectively. Similar results for microcells were published by M. Paire et al. with initial efficiencies at 1 sun between 12.8 and 14.5% [9,10,12].

To qualify the relation between active cell width (ACW) and the interconnection-zone width (ICW) better, their geometrical ratio is introduced as new analyzing parameter (ACW/ICW-ratio). Large ratios stand for a dominance of active cell area, small ratios stand for a dominance of the ICW. In figure 3, the total area based and the active area based efficiencies are plotted together in relation to this new parameter. Now, one can notice a stable scattering around 14.0 +/- 1.0% active area efficiency as long as the ACW/ICW-ratio is higher than 2.5. For cells with lower ratio, the total area as well as the active area based efficiencies started to decrease significantly. For ACW/ICW-ratios below 1.0, the active area based efficiencies descend below 10%. As a consequence of this analysis, it is concluded that the P-scribe based interconnection zone interferes the ACW at least 2 to 3 times of its own width. As a consequence, this would denotes for the preparation of lamellar, P-scribe based interconnected microcells that the limiting cell width will be about 600-700 µm, considering recent P-scribe interconnect dimensions with total distances between 250-300 µm (P1 to P3) [28].

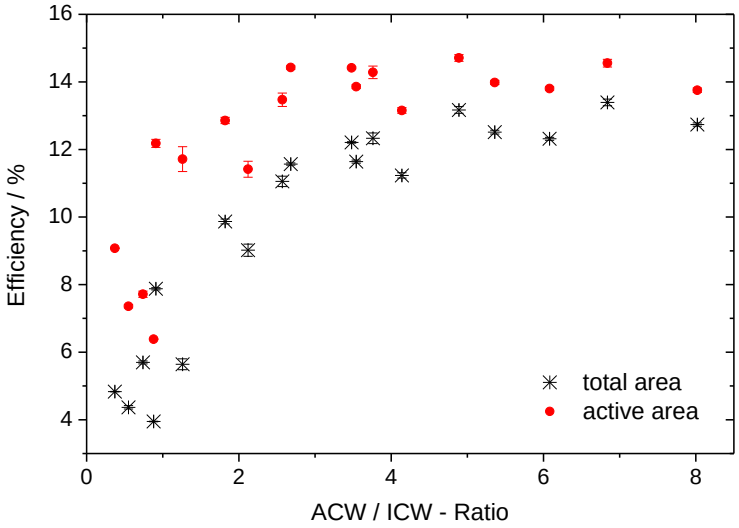

Figure 3: Plot of total and active area based conversion efficiencies of lamellar microcells against their geometrical ratio between active cell width (ACW) and interconnection zone width (ICW).

Before the results were discussed in more detail, the interest and typical properties of monolithic, P-scribe based interconnects are explained. The advantages of the P-scribe based contact design pattern for industrial thin film solar modules are shadow free surfaces and a cost effective in-line processing [28]. However, it also lacks from some disadvantages. First, the P1-scribe is filled with the photoconductive semiconductor Cu(In,Ga)Se_2, what influences the parallel resistance of the cell (R_p). Second, the highly conductive ZnO:Al filled in the P2-scribe creates shunted and therefore inactive cell areas. And third, the cell´s series resistance R_s is not only influenced by the conductivity of the front contact material but also by the final lateral cell dimension. These circumstances inevitably cause lower conversion efficiencies for monolithically interconnected cells compared to their counterparts with a finger-like contact grid. This could be confirmed in the experiments (fig.: 2). What is that supposed to mean for microcells now? Because of the fact, that at 1 sun the total area based current densities will be lower for microcells than for macroscopic ones, it is expected, that microcells suffer stronger from all kind of peripheral charge carrier loss mechanism, like shunts, barriers and other recombination center. In addition, the screening effect for electrical defects will also be reduced and the relative fraction of losses will increase. High parallel cell resistances as well as preferably defect free layer stacks can be a solution. The observed partial recovery of efficiency in case of microcells after increasing the P1-scribe width supports this thesis. How much the supply of concentrated light and the within increased photocurrents can countermand these effects is investigated and discussed in chapter 4.2.

Contrary to the challenges for high R_p-values, the microcell design comes along with a reduction of lateral distances for current transportation, what should finally result in lower R_s. And in fact, the determined averaged series resistances R_s decreased in series A by almost 8% from 2.4 to 2.2 Ohm after lowering the ACW from 1900 to 1000 µm. In contrast, the averaged R_s values rose with increasing P1-scribe width from 2.4 Ohm for series A cells to 3.2 Ohms for series D-cells with 1900 µm ACW. For 200 and 500 µm ACW-sized microcells these trends did not appeared that clearly, although the internal IC-dimension between P1- and P3-scribe was fixed for all investigated series. One explanation may be that structural defects in the P1-scribe caused superposed influences. The importance of passivated edges in case of microcells is also shown in [12].

The observed trends may be a special feature for lamellar, P-scribe based thin film solar cells. M. Paire et al. published contrary results for point-shaped Cu(In,Ga)Se_2 cells, but cite a similar behavior for Si- and GaAs-based microcells [12]. The importance of edge and surface passivation is also highlighted [29]. For future cell designs equipped with similar interconnects, the ACW should be at least 3-times larger than the ICW-zone. Considering a P1-scribe width of 70 µm, what showed already a significant improvement in the experiments, a P2-scribe width of 40 µm together with a P1P2- and P2P3-distance of 80 µm, what correspond to recent standards and technically possible solutions for mechanical scribing processes, the optimum in cell minimization would be then between 600 and 700 µm ACW.

Summarizing the experimental results observed for macroscopic and microscopic lamellar cells at STC-conditions, it is concluded that the P-scribe based interconnection zone has a significant influence on the cell performance, particularly in the case of microcells. Altered conditions in the internal parallel- and series resistances are made primarily responsible for the observed trends.

4.2 Lamellar microcells at concentrated light test conditions (CLTC)

A selection of cells was chosen to investigate their performance under concentrated light. The question to be solved was: can the re-increased photocurrents compensate the losses observed at standard test conditions completely? The under concentration increased photon flux density does not only influence I_{sc} and U_{oc} (eq. 1.2, 1.3), but also the electric conditions in the device start to change, what finally results in different bulk conductivities and screening lengths for electric potentials and shunts [9, 30-32]. In figure 4, the relative changes in U_{oc} are plotted against the logarithm of the light concentration factor for 3 differently sized lamellar cells out of series C. The U_{oc}-trend of a dot-shaped micro cell with 750 µm active area radius is also shown for comparison.

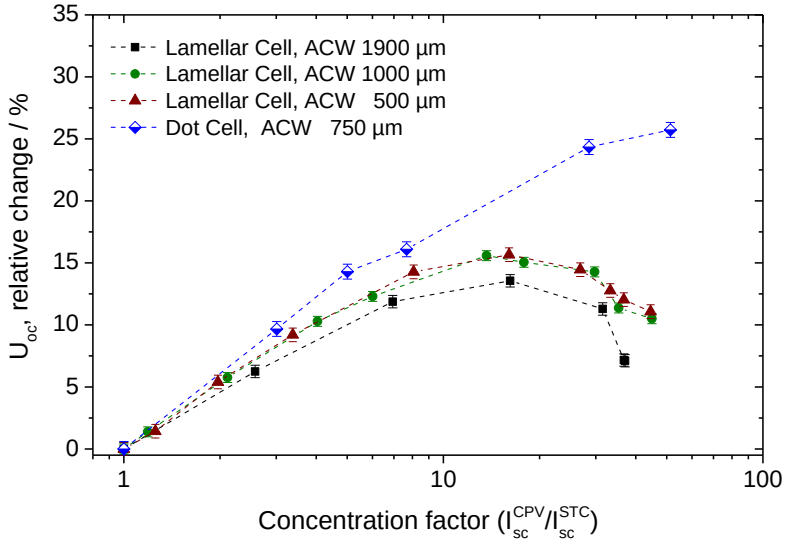

Figure 4: Trend of the relative change in open circuit voltage against the concentration factor (log-plot) for differently sized lamellar cells out of series C. The trend observed for dot-shaped microcells without P-scribe based interconnects is given in blue color.

Three different regimes in the U_{oc} versus log C-plot could be deduced for the lamellar microcells. In the first regime, at low concentration level between 1 and 6 suns, the U_{oc}-values rose linearly for all investigated cell dimensions, like expected from equation 1.3. For slightly higher concentration levels,

the U_{oc} was still increasing, but their slopes decreased. In the third regime, the U_{oc}-values did not increase anymore and started to drop for concentration levels above 20 suns. The lamellar microcells with 500 and 1000 µm ACW showed the best relative increase in U_{oc} with plus 15.7 and plus 15.6% at 16.0 and 13.6-times concentration, respectively. In absolute values, the U_{oc}-values increased by more than 58 mV to the measured optimum of 615 mV. Considering a temperature based correction (chapter 3), the U_{oc}-optimum rose by 87 mV to finally 645 mV. For the 750 µm ACW dot-shaped microcells, the U_{oc}-maximum could not be observed up to 51-times concentration. The relative increase was 25.7% at 51.0 suns corresponding to 642 mV measured and 693 mV recalculated for STC-temperature conditions. Contrary to the lamellar cells, no significant decline in the U_{oc}-trend could be observed between 15 and 51 suns for small dot shaped microcells. Whereas the U_{oc}-increase is related to an increased number of photons and the within enhanced Fermi-level splitting, the U_{oc}-reduction in the third regime is assigned to resistance based losses that counterbalance the enhancement. Local changes in the light spectrum caused by the concentration with lenses, that can also influence the U_{oc} in principle, are excluded, because of the usage of lenses that were optimized for low spherical and chromatic aberrations. The influence of temperature on the population of states and hence the U_{oc} is considered by using a temperature coefficient that is described in detail in chapter 3. Similar thermal conditions are expected for all investigated cell-types. Due to the fact, that the absorber material was prepared in one batch, the recognized slightly different slopes in U_{oc}-growth are related to different saturation currents and their relation to the cell- and contact area. The smaller the cell- and contact area, the lower can be I_0 in case of an ideal, defect free absorber layer in the active cell region.

Analyzing the maximum cell power P_{mp} in dependence of the light concentration, similar trends could be observed like for the U_{oc}. For low concentration level, the experimentally observed P_{mp}-values followed the ideal linear trend (eq. 1.4), whereas for high concentration level the P_{mp}-trend curves started to depart. Again, cells with the largest ACW started to deviate first. For the lamellar microcells with 500 µm ACW, the normalized cell power increased from 10.7 to 551 mW/cm^2 at 44.5x concentration. In the matter of saving material, the Cu(In,Ga)Se_2 deposited area could therefore be reduced by a factor of 51 (ACW). For the dot-shaped microcells the power density increased from 12.8 to 776 mW/cm^2 at 44.5x and to 902 mW/cm^2 at 51x concentration, realizing a theoretical material saving factor of 61 and 70, respectively. In practice and for lamellar Cu(In,Ga)Se_2 solar cells with P-scribe interconnects in particular, the real convertible area reduction would be significantly lower. First of all, a band of 200 to 300 µm deposited Cu(In,Ga)Se_2 film will be needed in addition to establish the recent standard P-scribe based interconnection zone [28]. This band-width corresponds to 40 and 60% of a 500 µm ACW microcell. Consequently, the realizable area reduction will drop between 20 to 30 times, respectively. Considering inevitable additional losses caused by the interplay of several cells and strings in the final solar module, that typically account for 5 to 15% of the maximum cell power [3], it is expected that the material saving factors will reduce further to 15 to 25-times. Therefore, new ways are needed to contact lamellar microcells without large area consuming ICW-zones.

In figure 5 the cell efficiencies observed for 1900, 1000 and 500 µm sized lamellar cells out of series C and for a 750 µm sized dot-shaped cell are plotted against the logarithm of the light concentration factor. The efficiencies rose steeply and almost linear for low concentrations, saturated at a certain peak level and started to decline thereafter. The lower the lateral cell dimension, the higher was the concentration level for the efficiency peak position. For the 1900, 1000 and 500 µm ACW sized lamellar cells, the optimum was observed with 14.8% at 2.6x, 15.0% at 6.0x and 14.6% at 8.0x concentration, respectively. For the dot-shaped solar cell the maximum efficiency could not be identified between 1 and 51 times light concentration. The best measured efficiency was 17.6% at 51 suns. Most influencing parameter for the reduced efficiencies at high concentrations was always an

intense drop in *FF*, whose value was reduced from 60-70% to less than 50% depending on the microcell size. Its drop always sets in, before the U_{oc}-values started to decline.

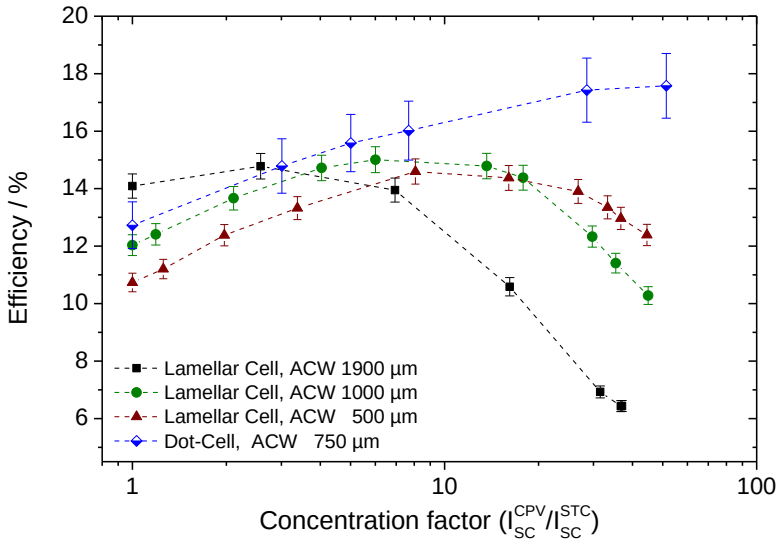

Figure 5: Plot of the active area based conversion efficiency of lamellar cells out of series C and of a 750 µm sized dot-shaped cell against the light concentration factor (log-plot). All efficiencies were corrected to 298.1 K.

In relation to the values observed at 1 sun, the efficiency of the lamellar microcells increased by 0.7%, 3.0% and 3.8% absolute and 4.9%, 24.7% and 35.9% relative. In case of the dot-shaped microcells the averaged efficiency increased by 4.8% absolute and 38.1% relative. Analyzing the benefit of "cell-minimization" selectively for the lamellar, P-scribe based interconnected cell series, the gain in efficiency is rather low. In the investigated CLTC-series, the 1000 µm ACW sized cells perform in average only 1.5% (0.23% absolute) better than their macroscopic references with 1900 µm ACW. For the 500 µm ACW cells the maximum efficiency is in contrast 0.20% absolute lower. Taking the macroscopic cells equipped with a finger-like metal grid and an average efficiency of 15.6% at 1 sun (table 1) as reference, the relative improvement was positive only for the dot-shaped microcells and showed 12.8% relative increase. But particular for the last given relation, it should be considered that a comparison of different contact methods and contact grids cannot be done by simple analogy. New key-parameters are needed to quantify the different losses and gains in series- and parallel resistances and in particular their antagonize behavior at concentrated light in case of different grid-types and contact designs.

In the experiments with concentrated light significant changes were observed for R_s and R_p for both types of microcell geometries and contact designs. The averaged R_p dropped with increasing concentration from 2500 to 3000 Ohm to values below 150 Ohm. A likewise trend was observed for the series resistances. Starting with values around 4.5 to 5.5 Ohm at 1 sun, the averaged R_s-values decreased to 2.5 and 3.2 Ohm under concentration. Both trends can explain the observed changes in *FF* and were related first to a light induced increase in conductivity and second to changes in the inner electrical fields of the diode. Both effects are expected and well known for photoactive semiconductors and $Cu(In,Ga)Se_2$ in particular [9, 30-33]. It is further to consider, that the finally estimated R_s and R_p values reflect the sum of different particular single parallel- and series resistances that vary on the material, contacts and geometry used and that may change differently during concentration. M. Paire et al. discuss in addition a reduction of R_s related to a shift into the "high injection regime" [10]. Own

tests in that field showed a change in specific resistivity by one order of magnitude from 2885 Ohm*cm at 1 sun to 246 Ohm*cm at 33 suns. A changed charging of internal defects is also highly reasonable for the observed findings [31,32].

In addition, it is to consider that high current flows led the difference between the voltage across the pn-junction (U_{pn}) and the voltage, present at the cell contacts (U_{con}), successively increase [33]. As a consequence of the relation $U_{pn}=U_{con} - I*R_s$, where the current shows a negative quantity, the voltage at the pn-junction will became larger than the terminal voltage at the contacts. It is argued now, that this effect will cause a switch of the diode in forward direction. Because of the grain like structure present in CIGSe solar cells and the known gradients in the Gallium depth-profile, it is assumed, that this switch take place differently for certain grains or regions of the solar cell. The larger the series resistance in the cell, the more distinctive will these effects be. As a consequence, new shunt paths were created at high concentration level and insufficient charge transport. These arguments may verify the observed stronger relative change in R_p than in R_s. But it may also be, that the chosen axis intercept between 0.85 and 0.95 V was not sufficient enough for a correct determination of R_s or that other effects in the device influence the R_s-determination.

To revisit the question in the beginning of chapter 4.2, it can be stated by the experimental results, that light concentration can compensate successfully losses that were caused by the changed ratio between active cell area (ACW) and interconnection zone (ICW) in case of microcells. But it also shows that each cell design has its own optimum in minimization. The comparison between lamellar- and dot-shaped microcells showed, that the last mentioned cell- and contact design clearly benefit from the lower series resistances and the structurally related lower number of shunt paths. For dot-shaped microcells, the concentration profile of U_{oc} and efficiency obeyed longer the ideal behavior and the limiting threshold region is reached at significant higher concentration levels. But, the global trends observed for large and small dot-shaped microcells were the same like for lamellar designed and monolithically interconnected microcells. The smaller the microcell, the higher was the concentration level for the optimum in efficiency and exceeding a certain level the minimization became disadvantageous for the chosen cell- and contact design at all.

4.3 Simulation of lamellar microcell performance at concentrated light test conditions (CLTC)

The influence of series- and parallel resistances on the cell performance is reflected in the fill factor *FF* of a solar cell (chapter 2, eq. 1.4). To predict the performance of solar cells at different CLTC-conditions, a *FF*-based simulation routine is introduced and discussed in the following section. It is based upon equations 1.2 to 1.6. A sequence of the calculation and simulation is shown in figure 6.

Measured IV-data of a microcell with 1000 µm ACW were used to implement the dependence of the saturation current on the light concentration into the model. In addition, the experimentally observed temperature relation (section 3) and the separately calculated values for R_s and R_p are included as initial "input"-parameters. The values for R_s and R_p were estimated by applying a linear fit-procedure to the IV-curves of illuminated cells in the 1st and 4th quadrant, respectively (chapter 3). The "input"-parameter diode factor *n* was determined by equation 1.1 at 1 sun illumination density and used as fixed value for higher concentrations. In order to simplify the calculations, no change in the primary recombination is presumed for this assumption. The open circuit voltage was calculated by using equation 1.3, considering the concentration dependent saturation current relation and the absorber

material related temperature coefficient (chapter 3). By using these "input"-parameter, the solar cell performance can now be calculated for several concentration level by an iterative solution of equation 1.6, wherefrom finally the *FF*, the maximum cell power and the conversion efficiency can be determined by equation 1.5 and 1.4, respectively. On basis of this model, new cell designs can now be simulated for different CLTC-conditions, when the contact- and material properties are similar.

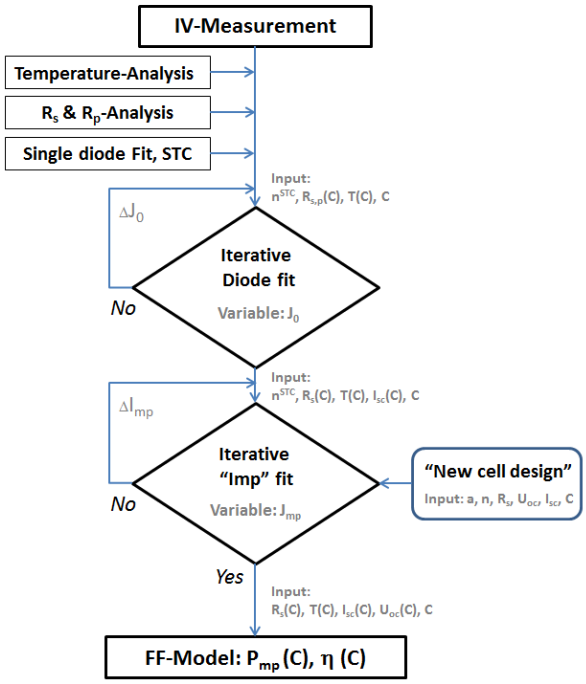

Figure 6: Calculation sequence in order to simulate the IV-characteristic of lamellar microcells at different concentration level.

The simulation results can be found in figure 7, where the calculated conversion efficiencies are compared to the experimentally determined ones including a variation of artificially increased and decreased series resistances. Looking for the simulation results with an initial R_s-value of 5.4 Ohm, the efficiency is slightly overestimated between 1 and 1.5 suns and underestimated between 3 and 20 suns. The relative deviation varies between 6.0% and -4.0 to -5.0% relative for low and high concentration level, respectively. Increasing the value of R_s leads to an almost similar behavior at low concentration level but lowers the overall efficiencies and intensifies the decline in case of higher concentration level. Contrary to this, the reduction of R_s results in higher overall efficiencies and lowers its decline for high concentration level (fig. 7). For cells with R_s-values below 0.5 Ohm, the most influencing parameter changed from *FF* to the negative temperature coefficient of the open circuit voltage that finally deteriorates the conversion efficiency.

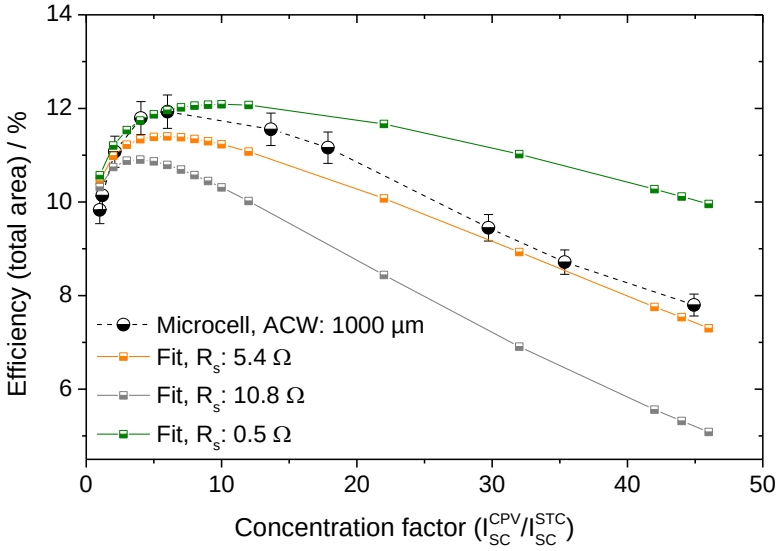

Figure 7: Simulation of the conversion efficiency based on the *FF*-model introduced in chapter 1.1 and 4.3. Experimental raw data of a lamellar microcell with 1000 µm ACW were used for the initial setup.

The addressed inaccuracy in the simulation is caused by several assumptions. First, the diode factor *n* was fixed in the calculations of the saturation dark current and for the *FF*-model (fig. 6). Second, the influence of any parallel resistances is in this first basic approach for reason of simplicity neglected so far. And third, the iterative fitting of the primary IV-curves results in different fit quality during the CLTC-series. With increasing light concentration the fit quality drops significantly, apparent with decreasing R^2 (chi-square) values from 0.99 to 0.78. As a consequence, the estimated saturation dark current values lack in accuracy what will influence of course all constitutive calculations. Nevertheless, the general trend of the cell power and the conversion efficiency on the light concentration can be calculated in a qualitative way. This can help to simulate and optimize future cell geometries in a faster way.

5. Conclusion

The experimental series with differently sized lamellar, monolithically interconnected solar cells showed that the open circuit voltage, the power density and the conversion efficiency can be increased by concentrated light. But the improvement strongly depends on the chosen cell geometry, the contact method and the electrical material properties. In the experimental series with concentrated white light, the conversion efficiency could be increased by more than 3.8 % absolute for the lamellar microcells and more than 4.8% absolute for dot-shaped microcells in relation to their performances at STC-conditions. The maximum power density stepped up by a factor of 51 and 70-times, respectively. In the comparison between micro- and macro-cells, the application of concentrated light could increase the efficiency by 0.9% absolute for lamellar and by 1.3% absolute for dot-shaped microcells. The global trends observed between large and small microcells were the same for lamellar, monolithically interconnected and dot-shaped, ring-contacted solar cells. It is important to consider, that each cell- and contact design has its own optimum in minimization and light concentration.

The experimental and simulated data showed further that the widely industrially used CIGS cell design pattern cannot simply be adapted to prepare micro-concentrator CIGS solar modules. To improve the efficiency of microcells at STC- and CLTC-conditions, special attention should be paid to the series-

and parallel resistances of the device. Their optimization could be realized either by a change of the contact method itself [34,35] or by eliminating critical elements in the standard contact technique. Increasing the width of the P1-scribe could improve the performance of the lamellar microcells at STC- and CLTC-conditions, but amplitudes above 100 µm scribe width became unrealistic for real applications and uninteresting in favor of material saving aspects. New solutions to increase the parallel resistance and to minimize series resistances have to be found.

The experimental results clearly support, that a minimization of solar cells in combination with light concentrating elements can be a powerful option to develop higher conversion efficiencies in conjunction with a lowered material consumption. Future work will focus on the proposed optimization of the contact design, the investigation of material properties and the improvement of the *FF*-model in order to simulate micro-concentrator solar cells with more accuracy.

6. Acknowledgement

Financial support from the Helmholtz association for the young investigator group "Nanooptical concepts for PV" (VH-NG-928) is highly acknowledged. Carola Ferber and Michael Kirsch are acknowledged for the deposition of buffer- and contact layers.

7. References

[1] Kaneshiro J, Gaillard N, Rocheleau R., Miller E., Advances in copper-chalcopyrite thin films for solar energy conversion, Solar Energy Materials & Solar cells, 2010, 94, 12-16.

[2] M. Mauk, P. Sims, J. Rand, A. Barnett, Practical Handbook of Photovoltaics: Fundamentals and Applications, Chapter IB-4, Thin Silicon Solar Cells, 2012, 161-170.

[3] Green M.A., Emery K., Hishikawa Y., Warta W., Dunlop E.D., Solar cell efficiency tables (version 45), Progr. Photovolt. Res. Appl., 2015, 23, 1-9.

[4] Press Release, ZSW-Stuttgart, 22.09.2014, http://www.zsw-bw.de/uploads/media/pi12-2014-ZSW-WeltrekordCIGS.pdf.

[5] Atwater H., Polmann A., Kosten E., Callhahan D., Spinelli P., Eisler C., Escara M., Warmann E., Flowers C., Nanophotonic design principles for ultrahigh efficiency photovoltaics, AIP-Conference Proceedings, 2013, 17, 1519.

[6] Polmann A., Atwater H.A., Photonic design principles for ultrahigh-efficiency photovoltaics Nature Materials, 2012, 11, 174-177.

[7] Strümpel C., McCann M., Beaucarne B., Arkhipov V., Slaoui A., Svrcek V., del Canizo C.,Tobias I., Modifying the solar spectrum to enhance silicon solar cell efficiency - An overview of available materials, Solar Energy Materials & Solar Cells, 2007, 91, 238-249.

[8] Paire M., Lombez L., Guillemoles J.F., Lincot D., Toward microscale Cu(In,Ga)Se_2 solar cells for efficient conversion and optimized material usage: Theoretical evaluation, J. Applied Physics, 2010, 108, 034907-1 – 034907-7.

[9] Paire M., Lombez L., Donsanti F., Jubault M., Pere-Laperne N., Collin S., Perona A., Dollet A., Pelouard J.L., Lincot D., Guillemoles J.F., Cu(In,Ga)Se_2 photovoltaic microcells for high efficiency with reduced material usage, Proc. SPIE 8256, 2012, doi: 10.1117/12.908613.

[10] Paire M., Lombez L., Pere-Laperne N., Collin S., Pelouard J.L., Lincot D., Guillemoles J.F., Microscale solar cells for high concentration on polycrystallin Cu(In,Ga)Se_2 films, Appl. Physics Lett., 2011, 98, 264102-1 – 264102-3.

[11] Paire M., Shams A., Lombez L., Pere-Laperne N., Collin S., Pelouard J.L., Guillemoles J.F., Lincot D., Resistive and thermal scale effects for Cu(In, Ga)Se_2 polycrystalline thin film microcells under concentration, J. Energy & Environmental Science, 2011, 4, 4972-4977.

[12] Paire M., Lombez L., Donsanti F., Jubault M., Collin S., Cu(In,Ga)Se_2 microcells: High efficiency and low material consumption, J. Renewable Sustainable Energy, 2013, 5, 011202-1/5.

[13] Baker K.A., Karp J.H., Tremblay E.J., Hallas J.M., Ford J.E., Reactive self-tracking solar concentrators: concept, design, and initial materials characterization, J. Applied Optics, 2012, 51, 8, 1086-1094.

[14] Yoon J., Baca A.J., Il-Park S., Elvikis P., Geddes J.B., Li L., Kim R.H., Xiao J., Wang S., Ho-Kim T., Motala M.J., Ahn B.Y., Duoss E.B., Lewis J.A., Nuzzo R.G., Ferreira P.M., Huang Y., Rockett A., Rogers J.A., Ultrathin silicon solar microcells for semitransparent, mechanically flexible and microconcentrator module designs, Nature Materials, 2008, 7, 907-916.

[15] Karp J.H., Temblay E.J., Hallas J.M., Ford J.E., Orthogonal and secondary concentration in planar micro-optic solar collectors, J. Optics Express, 2011, 19, A673-A685.

[16] Kanayama M., Oku T., Akiyama T., Kanamori Y., Seo S., Takami J., Ohnishi Y., Ohtani Y., Murozono M., Microstructure Analysis and Properties of Anti-Reflection Thin Films for Spherical Silicon Solar Cells, J. Energy and Power Engineering, 2013, 5, 18-22.

[17] Kang D., Arab S., Cronin S.B., Li X., Rogers J.A., Carbon-doped GaAs single junction solar microcells grown in multilayer epitaxial assemblies, Appl. Phys. Lett., 2013, 102, 253902-1/5.

[18] Ward J.S., Ramanathan K., Hasoon F.S., Couth T.J., Keane J., Contreras M.A., Moriarty T., Noufi R.A., A 21.5% efficient Cu(In,Ga)Se_2 thin-film concentrator solar cell, Progr. Photovolt. Res. Appl. 2002, 10, 41-46.

[19] Brogren M., Wennerberg J., Kapper R., Karlsson B., Design of concentrating elements with CIS thin film solar cells for fa-cade integration, Solar Energy Materials & Solar Cells, 2003, 75, 567-575.

[20] Wennerberg J., Kessler J., Hedström J., Stolt L., Karlsson B., Rönnelid M., Thin Film PV Modules for Low-Concentrating Systems, J. Solar Energy, 2000, 69, 243-255.

[21] Goucher F.S., Pearson G.L., Sparks M., TEAL G.K., Shockley W., Theory and Experiment for a Germanium pn-Junction, Physical Review, 81, 1954, 637-638; Shockley W., Queisser H.J., Detailed Balance Limit of Efficiency of *p-n* Junction Solar Cells, J. Appl. Physics, 1961, 32, 510-519.

[22] Pulfrey D.L., On the Fill Factor of Solar Cells, J. Solid State Electronics, 1978, 21, 519-520.

[23] Taretto K., Soldera M., Troviano M., Accurate explicit equations for the fill factor of real solar cells - Applications to thin-film solar cells, Prog. Photovolt. Res. Appl., 2013, 21, 1489-1498.

[24] Rocheleau R.E., Miller E.L., Photoelectrochemical Production of Hydrogen: Engineering Loss Analysis, Int. J. Hydrogen Energy, 1997, 22, 8, 771.

[25] We would like to note here a correction of the original equation given in [19], where I_{mp} is printed in the denominator instead of I_0.

[26] Kaufmann C.A., Neisser A., Klenk R., Scheer R., Transfer of Cu (In, Ga)Se_2 thin film solar cells to flexible substrates using an in situ process control, Thins Solid Films, 2005, 480, 515-519.

[27] IV-T measurements of macroscopic cells out of the same batch, Temperature-coefficient 280 to 320 K: -0,239%/K.

[28] Westin P.O., Zimmermann U., Ruth M., Edoff M., Next generation interconnective laser patterning of CIGS thin film modules, Solar Energy Materials & Solar cells, 2011, 95, 1062-1068.

[29] Paire M., Lombez L., Donsanti F., Jubault M., Collin S., Pelouard J.L., Lincot D., Guillemoles J.F., Thin-film microcells: a new generation of photovoltaic devices, SPIE-Newsroom, 10.1117/2.1201305.004808.

[30] Tinocco T., Rincon C., Omintero M., Charebois A., Tauc J., Photoconductivity Spectrum, Deformation Potentials and Effective Masses of Carriers for the Chalcopyrite Semiconductor Alloy $CuIn_{0.6}Ga_{0.4}Se_2$, Solid State Comm., 1993, 87, 77.

[31] Igalson M., Urbaniak A., Krzysztopa A., Aida Y., Caballero R., Edoff M., Siebentritt S., Sub-bandgap photoconductivity and photocapacitance in CIGS thin films and devices, Thin Solid Films, 2001, 519, 7489-7492.

[32] Guillemoles J.F., Stability of Cu(In,Ga)Se_2 solar cells: a thermodynamic approach, Thin Solid Films, 2000, 361, 338-345.

[33] Wolf M., Rauschenbauch H., Series resistance effects on solar cell measurements, Adv. Energy Conversion, 1963, 3, 455-479.

[34] Wagner M., Würz R., Kessler F., Post-Monolithic Interconnection of CIGS Solar Cells, 24th. EU-PVSec Conference Proceedings, 2009, 2986-2988.

[35] Westin P.O., Wätjen J.T., Zimmermann U., Edoff M., Microanalysis of laser micro-welded interconnections in CIGS PV modules, Solar Energy Materials & Solar cells, 2012, 98, 172-178.